J Mater Sci (2011) 46:3452–3463
DOI 10.1007/s10853-011-5250-0

Phonon dispersion and specific heat in *trans* 1,4, poly (2,3-dimethylbutadiene)

Archana Gupta · Saba Bee · Parag Agarwal · Poonam Tandon · Vishwambhar Dayal Gupta

Received: 11 November 2010 / Accepted: 6 January 2011 / Published online: 1 February 2011

Abstract A comprehensive study of the normal modes and their dispersion for *trans* 1,4-poly (2,3 dimethylbutadiene) is described in the reduced zone scheme using Wilson's GF matrix method as modified by Higg's for an infinite polymeric chain. Urey Bradley force field is obtained by least square fitting of the observed IR and Raman bands. Optically active frequencies corresponding to the zone center and zone boundary are identified and discussed. Some of the characteristic features of dispersion curves are repulsion accompanied by exchange of character and Von Hove type singularities. The evaluation of normal modes and their dispersion has been taken to logical conclusion by calculating the heat capacity as a function of temperature. Specific heat has been obtained from dispersion curves via density of states in the range 10–400 K using Debye's relation. The predictive values of specific heat show a typical variation for an one dimensional polymeric system.

Introduction

Polymers are capable of existing in a variety of conformations that give rise to a composite/complex spectrum difficult to unravel. The IR spectrum characterizes the vibrational modes of the molecule and enfolds a lot of information on chain structure. For polymers, it includes analyzing and identifying polymeric complexities and subtle structural variations such as tacticity and neighboring group interactions [1, 2]. Raman spectroscopy can also provide exquisite structural insights into macromolecules like polymers and biological systems such as enzymes and nucleic acid–protein complexes as the Raman Effect involves an intimate interplay among the atomic positions, electron distribution, and intermolecular forces [3, 4]. The combined use of IR and Raman spectroscopies provides useful information and these spectroscopies are powerful tools in the arsenal of polymer scientists. In general, the IR absorption, Raman spectrum, and inelastic neutron scattering from polymeric systems are very complex and can not be analyzed without proper knowledge of dispersion curves. Lack of this information in many polymeric systems has been responsible for incomplete understanding of their spectra. Through the dispersion curves one can not only obtain information on the extent of coupling along the chain, but also the origin of both symmetry dependent and symmetry-independent spectral features. Further, the phonon dispersion curves can be used to calculate the density of states, which are important in the analysis of thermodynamically important properties of a polymer and can be used to correlate the macroscopic properties viz. heat capacity, entropy, enthalpy to the microscopic behavior of a crystal. In continuation of our study in a variety of polymeric systems [5–8] in this communication, we report a comprehensive study of the normal mode analysis of poly 2,3-dimethylbutadiene (PDMB) using Urey Bradley force field (UBFF). In addition, phonon dispersion and heat capacity from the density of states derived from the dispersion curves are also reported.

A. Gupta (✉) · S. Bee · P. Agarwal
Department of Applied Physics, Institute of Engineering and Technology, M. J. P. Rohilkhand University, Bareilly, India
e-mail: drarchana.physics@gmail.com

P. Tandon · V. D. Gupta
Department of Physics, University of Lucknow, Lucknow, India

The monomer 2,3 dimethylbutadiene (DMBD) was the first to be used for the industrial production of synthetic rubber known as "methyl rubber" [9, 10]. The stereo specific polymerization of 2,3-DMBD monomer into long chains can be caused by irradiation [11–14]. Recently Cataldo et al. [15] have synthesized PDMB by the radiation-induced inclusion polymerization technique in which 2,3 dimethylbutadiene was induced as a clathrate in the channels of thiourea crystals. They have compared the microstructure of PDMB obtained by inclusion polymerization to that obtained by radiation polymerization in bulk and emulsion polymerization with a free radical initiator and have shown that PDMB obtained by inclusion polymerization in thiourea clathrate is characterized by an extremely high 1,4 *trans* content. The complete absence of 1,4 *cis* units is suggested by the absence of the band at 1200 cm^{-1} in FTIR spectra, while the bands at 1151 and 1223 cm^{-1} are associated to the *trans* 1,4 content.

The normal mode analysis of PDMB has been reported by Petcavich and Coleman [16] using the valence force field that does not take into account non-bonded interactions. One of the infirmities of their study is the use of the same force field for both the molecules polyisoprene and polydimethylbutadiene. The difference between the two is the presence of hydrogen attached to the carbon in one and methyl group in the other. This will cause local perturbations extending at best up to the nearest neighbors. Further, no use has been made of dispersion curves in obtaining thermodynamic parameters. Thus, for a complete understanding of the vibrational dynamics a fresh look at PDMB is necessary. Here we have re-examined the phonon dispersion profiles of PDMB in *trans* form using UBFF [17] and have attempted to remove the infirmities as far as possible. The UBFF is more comprehensive than the valence force field. The UBFF has some merits over others:

1. Relatively less parameter are required to express the potential energy
2. No quadratic cross terms are included in the potential energy expression. The interaction between non-bonded atoms includes these terms
3. Arbitrariness in choosing the force constants is reduced.

The normal mode frequencies obtained are in a better agreement with the observed IR and Raman data [15, 16] than those reported by the previous workers [16]. These calculations also lead to some new assignments. The evaluation of normal modes and their dispersion has been taken to logical conclusion by calculating the heat capacity as a function of temperature. To the best of our knowledge, such detailed studies leading to correlation between the microscopic behavior and the macroscopic properties have not been reported yet.

Theory

Calculation of normal mode frequencies

The calculation of normal frequencies has been carried out according to Wilson's GF matrix method [18] as modified by Higg's [19] for an infinite chain. This method consists of writing inverse kinetic energy matrix G and the potential energy matrix F in terms of internal coordinates R. In the case of an infinite isolated helical polymer, there are an infinite number of internal coordinates which lead to G and F matrices of infinite order. Due to the screw symmetry of the polymer, a transformation similar to that given by Born and Von Karman can be performed which reduces the infinite problem to finite dimensions.

The transformation consists of defining a set of symmetry coordinates

$$S(\delta) = \sum_{s=-\infty}^{\infty} R^n \exp(is\delta),$$

where δ is the vibrational phase difference between the corresponding modes of the adjacent residue units.

The elements of the $G(\delta)$ and the $F(\delta)$ matrices have the form

$$G_{ik}(\delta) = \sum_{s=-\infty}^{\infty} G_{ik}^{s} \exp(is\delta),$$

$$F_{ik}(\delta) = \sum_{s=-\infty}^{\infty} F_{ik}^{s} \exp(is\delta).$$

The vibrational secular equation that gives normal mode frequencies and their dispersion as a function of phase angles has the form

$$|G(\delta)F(\delta) - \lambda(\delta)I| = 0 \qquad 0 \leq \delta \leq \pi. \tag{1}$$

The vibration frequencies $v(\delta)$ (in cm^{-1}) are related to the eigen values $\lambda(\delta)$ by the following relation:

$$\lambda(\delta) = 4\pi^2 c^2 v^2(\delta). \tag{2}$$

For any given phase difference δ (other than 0 or л), the $G(\delta)$ and the $F(\delta)$ matrices are complex. In order to avoid the difficulties involved in handling complex numbers, methods have been devised to transform the complex matrices into equivalent real matrices by constructing suitable linear combinations of the coordinates. One method of transforming a complex matrix to its real matrix equivalent is through a similarity transformation. It can be shown that any complex matrix H = M + iN can be replaced by the real one

$$\begin{pmatrix} M & -N \\ N & M \end{pmatrix}.$$

In this case, we can write $G(\delta) = G^R(\delta) + iG^I(\delta)$ and $F(\delta) = F^R(\delta) + iF^I(\delta)$, where $G^R(\delta)$, $F^R(\delta)$, $G^I(\delta)$, $F^I(\delta)$ are real and imaginary parts of $G(\delta)$ and $F(\delta)$.

The product $H(\delta) = G(\delta)\,F(\delta)$ becomes:

$$H(\delta) = \begin{pmatrix} G^R(\delta) & -G^I(\delta) \\ G^I(\delta) & G^R(\delta) \end{pmatrix} \times \begin{pmatrix} F^R(\delta) & -F^I(\delta) \\ F^I(\delta) & F^R(\delta) \end{pmatrix},$$

$$= \begin{pmatrix} H^R(\delta) & -H^I(\delta) \\ H^I(\delta) & H^R(\delta) \end{pmatrix}$$

where

$$H^R(\delta) = G^R(\delta)F^R(\delta) - G^I(\delta)F^I(\delta),$$

$$H^I(\delta) = G^R(\delta)F^I(\delta) + G^I(\delta)F^R(\delta),$$

The matrix $H(\delta)$ now has dimensions $2N \times 2N$. The eigenvalues therefore occur in pairs of equal values. The difficulty of dealing with complex numbers is thus avoided.

The use of the type of force field is generally the matter of one's chemical experience and intuition [20]. Potential energy for the UBFF used in this study can be written as

$$\begin{aligned} V = &\sum K_{j.k} r_{j,k}^{(m)} \left(\Delta r_{j,k}^{(m)}\right) + K_{j,k}\left(\Delta r_{j,k}^{(m)}\right)^2/2 \\ &+ \sum H'_{i,j,k} r_{i,j}^{(m)} r_{j,k}^{(m)} \left(\Delta\alpha_{i,j,k}^{(m)}\right) + H_{i,j,k} r_{j,k}^{(m)} \left(\Delta\alpha_{i,j,k}^{(m)}\right)^2/2 \\ &+ \sum F'_{i,k} q_{i,k}^{(m)} \left(q_{i,k}^{(m)}\right) + F_{i,k}\left(\Delta q_{i,k}^{(m)}\right)^2/2 \\ &+ \sum K_j^{\tau} \left(\Delta\tau_j\right)^2 + \sum K_j^{\omega} \left(\Delta\omega_j\right)^2, \end{aligned}$$

where the symbols have their usual meanings. The primed quantities are introduced as internal tensions. Non-bonded interactions involve attraction and repulsion of atoms due to *n*th overlap of their electron shells. These effects are usually expressed by the 6-exp or 6–12 type potentials. The tension terms are assumed to be zero.

Force constant evaluation

The force constants were obtained by the least square fitting. In order to obtain the "best fit" with the observed frequencies, the following procedure was adopted. Initially, approximate force constants were transferred from *β-trans*-1,4 polyisoprene [21]. Thus, starting with the approximate F matrix F_0 and the observed frequencies λ_{obs} (related through a constant), one can solve the secular matrix equation:

$$GF_0L_0 = L_0\lambda_0. \tag{3}$$

Let $\Delta\lambda_i = \lambda_{i\text{obs}} - \lambda_{i0}$ in the above equation, it can be shown that in the first order approximation

$$\Delta\lambda = j\Delta F$$

where j is computed from L_0. We wish to compute the corrections to F_0 so that the errors $\Delta\lambda$ are minimized. We use the theory of least square and calculate

$$j'p\Delta\lambda = (j'pj)\Delta F, \tag{4}$$

where p is a weighting matrix and j' is the transpose of j. The solution to this equation is obtained by inverting $(j'pj)$ to give

$$\Delta F = (jpj)^{-1}jp\Delta\lambda. \tag{5}$$

If the number of frequencies is greater than the number of matrix elements, the matrix $j'pj$ should be nonsingular and we obtain the correction ΔF which will minimize the sum of weighted squares of the residuals. If the corrections ΔF are fairly large, the linear relation between force constant and frequency term in the matrix Eq. 3 breaks down. In such a situation, further refinement using higher order terms in Taylor's series expansion of $\Delta\lambda_i$ is needed. This procedure was developed by Kings et al. [22].

Calculation of heat capacity

Dispersion curves can be used to calculate the specific heat of a system. For an one-dimensional system the density of state function or the frequency distribution function expresses the way energy is distributed among the various branches of normal modes in the crystal. It is calculated from the relation

$$g(v) = \sum \left[\left(\partial v_j/\partial\delta\right)^{-1}\right]_{vj(\delta)=vj}. \tag{6}$$

The sum is over all the branches j. If we consider a solid as an assembly of harmonic oscillators, the frequency distribution $g(v)$ is equivalent to a partition function. The constant volume heat capacity can be calculated using Debye's relation

$$\begin{aligned} C_v = &\sum g(v_j) kN_A (hv_j/kT)^2 \\ &\times \left[\exp(hv_j/kT)/\{\exp(hv_j/kT) - 1\}^2\right] \end{aligned} \tag{7}$$

with $g(v_i)\mathrm{d}v_i = 1$.

Results and discussion

Figure 1 represents the chemical repeat unit of PDMB. It has 16 atoms that give rise to 48-4 optical modes. The four modes for which $\omega \to 0$ as $\delta \to 0$ are called acoustic modes. Three of them are due to translations (one parallel and two perpendiculars to the chain axis) and one due to rotation around the chain axis. The unit cell is orthorhombic [$a = 9.13$, $b = 13.00$, c (fiber axis) $= 4.70$ Å] with a space group of $Pna2_1$, four chains per unit cell [11]. The line group of an isolated chain of PDMB is isomorphous to the point group C_i. The 44 optically active modes are distributed between two symmetry species Ag and Au. The Ag and Au species are Raman and IR active, respectively [16]. The translational repeat unit of PDMB has a center of

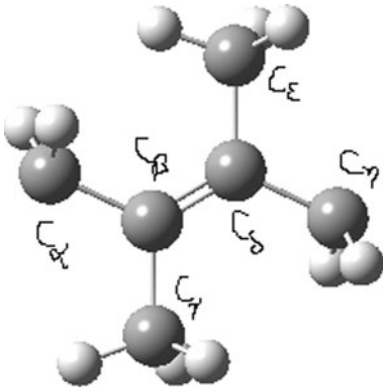

Fig. 1 One chemical repeat unit of PDMB

symmetry which implies mutual exclusion of the IR and Raman active modes. The experimental results confirm the same fact [16]. The Cartesian coordinates for an isolated chain have been calculated using the molecular parameters reported by Petcavich and Coleman [16]. Initially, approximate force constants were transferred from *β-trans*-1,4 polyisoprene [21] and then modified to obtain the "best fit" to the observed IR and Raman data [15, 16]. The final force constants along with the internal coordinates are given in Table 1. There is a wide difference in the force constants used by earlier workers [16] and the present one. This is obvious since the UBFF covers a wide potential surface including non-bonded interactions and tension terms. The same fact is widely reflected in the off diagonal elements of F-matrix and profile of the dispersion curves. The assignments are made on the basis of potential energy distribution, band position, band profile, intensity, and appearance/disappearance of similar modes placed in identical environment. The frequencies of vibration have been calculated at phase values ranging from 0 to π at intervals of 0.05π. The agreement between the observed and calculated frequencies is good. The matched frequencies along with their potential energy distribution (PED) are given in Tables 2 and 3. Since all the modes above 1450 cm^{-1} are non dispersive in nature, the dispersion curves are plotted only for the modes below 1450 cm^{-1}, in Figs. 2a and 3a. For simplicity, modes are discussed in two separate sections viz. non-dispersive modes and dispersive modes.

Non-dispersive modes

In general the non-dispersive modes are the ones that are highly localized in nature. The free stretching modes generally fall in this region, e.g., asymmetric and degenerate stretches of CH_3 group, asymmetric and symmetric stretches of CH_2 group. The calculated frequencies in the CH stretching region from 3100 to 2800 cm^{-1} are in good agreement with the observed bands. Since the molecule contains two CH_2 groups and two CH_3 groups in one repeat unit, the absorption bands appear in pairs. They are slightly away from each other because of their symmetry nature. The C=C stretching frequency is calculated at 1663 cm^{-1} and matched to the peak at 1665 cm^{-1} in the Raman spectra. These frequencies fall in the above-mentioned region [23]. The region from 1465 to 1335 cm^{-1} contains degenerate and symmetrical deformations of the CH_3 groups and the scissoring modes of the CH_2 groups. The

Table 1 Internal coordinates and Urey Bradley force constants

Internal coordinates	Force constants	Internal coordinates	Force constants
$\nu[C_\alpha–H]$	4.3	$\varphi[C_\beta=C_\delta–C_\varepsilon]$	0.68(0.300)
$\nu[C_\alpha–C_\beta]$	2.5	$\varphi[C_\beta=C_\delta–C_\eta]$	0.53(0.320)
$\nu[C_\beta–C_\gamma]$	2.7	$\varphi[C_\varepsilon–C_\delta–C_\eta]$	0.62(0.180)
$\nu[C_\gamma–H]$	4.29	$\varphi[C_\delta–C_\varepsilon–H]$	0.34(0.220)
$\nu[C_\beta=C_\delta]$	7.54	$\varphi[H–C_\varepsilon–H]$	0.412(0.287)
$\nu[C_\delta–C_\varepsilon]$	2.65	$\varphi[C_\delta–C_\eta–H]$	0.260(0.210)
$\nu[C_\varepsilon–H]$	4.25	$\varphi[C_\delta–C_\eta–C_\alpha]$	0.92(0.700)
$\nu[C_\delta–C_\eta]$	2.3	$\varphi[H–C_\eta–C_\alpha]$	0.52(0.180)
$\nu[C_\eta–H]$	4.3	$\varphi[H–C_\eta–H]$	0.43(0.210)
$\nu[C_\eta–C_\alpha]$	3.7	$\varphi[C_\eta–C_\alpha–H]$	0.37(0.210)
$\varphi[H–C_\alpha–H]$	0.40(0.295)	$\varphi[C_\eta–C_\alpha–C_\beta]$	0.93(0.620)
$\varphi[H–C_\alpha–C_\beta]$	0.31(0.200)	$\tau[C_\alpha–C_\beta]$	0.034
$\varphi[C_\alpha–C_\beta–C_\gamma]$	0.75(0.450)	$\tau[C_\beta–C_\gamma]$	0.015
$\varphi[C_\alpha–C_\beta=C_\delta]$	0.60(0.30)	$\tau[C_\beta=C_\delta]$	0.020
$\varphi[C_\gamma–C_\beta=C_\delta]$	0.64(0.220)	$\tau[C_\delta–C_\varepsilon]$	0.0425
$\varphi[C_\beta–C_\gamma–H]$	0.435(0.220)	$\tau[C_\delta–C_\eta]$	0.032
$\varphi[H–C_\gamma–H]$	0.39(0.287)	$\tau[C_\eta–C_\alpha]$	0.010

ν, φ and τ denote stretch, angle bend and torsion, respectively. Non-bonded force constants are given in parentheses. Unit of force constants for stretch is md/Å, for angle bend is md/Å rad^{-2}, and torsion is md Å

Table 2 Non-dispersive modes

Cal. freq.	Obs. freq.			Assignment (% PED) at $\delta = 0$
	IR[a]	Raman[a]	IR[b]	
2982	–	2980	–	$\nu[C_\gamma–H]$ (100)
2970	2970	–	2978	$\nu[C_\varepsilon–H]$ (100)
2942	2948	–	2944	$\nu[C_\alpha–H]$ (99)
2914	2918	–	2932	$\nu[C_\gamma–H]$ (99)
2912	–	2910	–	$\nu[C_\gamma–H]$ (100)
2909	–	2910	–	$\nu[C_\eta–H]$ (99)
2900	–	2910	–	$\nu[C_\varepsilon–H]$ (98)
2899	–	2910	–	$\nu[C_\varepsilon–H]$ (100)
2896	2860	–	2863	$\nu[C_\eta–H]$ (56) + $\nu[C_\alpha–H]$(42)
2892	–	2855	–	$\nu[C_\alpha–H]$ (58) + $\nu[C_\eta–H]$(41)
1663	–	1665	–	$\nu[C_\beta=C_\delta]$(75)
1465	1463	–	1459	$\varphi[H–C_\varepsilon–H]$(96)
1464	–	1462	–	$\varphi[H–C_\varepsilon–H]$(96)
1452	1445	–	1441	$\varphi[H–C_\eta–H]$(65) + $\varphi[H–C_\eta–C_\alpha]$(19) + $\nu[C_\eta–C_\alpha]$(10)
1442	1445	–	1441	$\varphi[H–C_\gamma–H]$(87) + $\varphi[H–C_\alpha–H]$(6)
1441	1445	–	1441	$\varphi[H–C_\gamma–H]$(94) + $\varphi[C_\beta–C_\gamma–H]$(5)
1438	–	1438	–	$\varphi[H–C_\alpha–H]$(70) + $\varphi[C_\eta–C_\alpha–H]$(9) + $\varphi[H–C_\gamma–H]$(7) + $\varphi[H–C_\alpha–C_\beta]$(5)
1383	–	1377	–	$\varphi[C_\beta–C_\gamma–H]$(47) + $\varphi[H–C_\gamma–H]$(43) + $\nu[C_\beta–C_\gamma]$(9)

All frequencies are in cm^{-1}

[a] Observed IR and Raman frequencies are from ref. [13]

[b] Observed IR frequencies are from ref. [12]

Only dominant PED's are given

calculated frequencies in this region match well with the observed data. The dispersion curves are essentially flat in this region. The two symmetrical deformation modes of methyl group are calculated at 1383 and 1336 cm^{-1} and are matched to the peaks at 1377 and 1331 cm^{-1}, respectively. One of these modes 1383 cm^{-1} is non dispersive. The lower frequency mode at 1336 cm^{-1} is initially non dispersive but around $\delta = 0.7\pi$, it suffers a repulsion with the dispersive mode at 1269 cm^{-1} comprising of various stretches and angle bends of the backbone. This repulsion is accompanied by exchange of characters. After this exchange, the former one becomes dispersive and the latter one assumes almost a constant value. The rocking of CH_3 groups is calculated at 954, 887, 878, and 817 cm^{-1}. Two modes at 878 and 954 cm^{-1} are non dispersive while the other two at 887 and 817 cm^{-1} are dispersive. Most of the frequencies of the CH_3 group occur in the same range as the corresponding ones in other synthetic polymers. A general comparison of the modes of CH_3 group in different polymers is shown in Table 4. This comparison is meaningful to the extent that the principle of group frequency supports the assignments. The scissoring modes of CH_2 group are calculated at 1452 and 1438 cm^{-1} and assigned to the peaks at 1445 and 1438 cm^{-1}, respectively. One of these frequencies does not match with that calculated by Petcavich and Coleman [16] at 1476 cm^{-1}. We have performed L vector analysis to ascertain the assignments of CH_3 and CH_2 group modes. There are some differences in the assignments of modes calculated by us and by Petcavich and Coleman [16]. This could have arisen because of different force fields. The UBFF in comparison to the valence force field is a better interactive field and emphasizes non-bonded interactions, which the valence force field does not. This can shift potential energy distribution and hence the dominant assignments may vary. All such modes which differ in assignments are listed in Table 5.

Dispersive modes

The modes, which are non-localized in nature and are strongly coupled, electrically, mechanically or both, show appreciable dispersion e.g., torsion modes are strongly coupled with the neighboring unit and are dispersive. The mode calculated at 1149 cm^{-1} comprises of wagging of both the CH_2 groups. It is matched to the peak at 1155 cm^{-1} observed in IR. This assignment differs with that of Petcavich and Coleman [16] who have shown the wagging of the

Table 3 Normal modes and their dispersion

Cal. freq.	Obs. freq.			Assignment (% PED) ($\delta = 0$)	Cal. freq.	Obs. freq.			Assignment (% PED) ($\delta = \pi$)
	IR[a]	Raman[a]	IR[b]			IR[a]	Raman[a]	IR[b]	
1336	–	1331	–	φ[H–C_ε–H](46) + φ[C_δ–C_ε–H](40) + ν[C_δ–C_ε](11)	1350	–	1331	–	ν[C_α–C_β](17)+ ν[C_η–C_α](17) + φ[H–C_η–H](12) + φ[C_η–C_α–H](11) + φ[C_δ–C_η–H](8) + φ[H–C_ε–H](5)
1269	1260	–	1257	ν[C_η–C_α](18) + ν[C_α–C_β](14) + ν[C_δ–C_η](11) + φ[C_η–C_α–H](10) + φ[C_δ–C_η–H](9) + φ[H–C_α–C_β](8) + φ[H–C_η–C_α](7)	1331	–	1331	–	φ[H–C_ε–H](42) + φ[C_δ–C_ε–H](37) + ν[C_δ–C_ε](7)
1227	1223	–	1223	ν[C_η–C_α](17) + ν[C_β–C_γ](10) + φ[H–C_α–C_β](8) + φ[C_α–C_β=C_δ](8) + φ[C_β=C_δ–C_ε](8) + ν[C_δ–C_ε](7) + φ[C_γ–C_β=C_δ](7) + φ[C_β=C_δ–C_η](7) + φ[C_δ–C_η–H](7)	1228	1223	–	1223	ν[C_δ–C_η](20) + ν[C_β–C_γ](10) + ν[C_δ–C_ε](9) + φ[C_β=C_δ–C_ε](9) + φ[C_α–C_β=C_δ](8) + φ[C_γ–C_β=C_δ](7) + φ[C_β=C_δ–C_η](7)
1149	1155	–	1151	φ[H–C_η–C_α](21) + φ[C_δ–C_η–H](18) + φ[H–C_α–C_β](14) + ν[C_α–C_β](13) + φ[C_η–C_α–H](12) + ν[C_δ–C_η](12)	1120	1155	–	1151	φ[H–C_η–C_α](41) + φ[C_δ–C_η–H](19) + φ[H–C_α–C_β](15) + φ[C_η–C_α–H](13)
1102	1095	–	–	φ[H–C_η–C_α](64) + φ[C_δ–C_η–H](13) + φ[C_η–C_α–H](9)	1095	1095	–	–	φ[H–C_η–C_α](47) + φ[C_η–C_α–H](14) + φ[C_δ–C_η–H](11) + φ[H–C_α–C_β](10)
1057	1050	–	1044	φ[C_η–C_α–H](39) + φ[H–C_α–C_β](28) + ν[C_δ–C_ε](9) + ν[C_β–C_γ](8) + φ[C_δ–C_η–H](6)	1065	1050	–	1044	ν[C_η–C_α](23) + ν[C_α–C_β](10) + φ[C_δ–C_η–C_α](10) + ν[C_δ–C_ε](9) + ν[C_η–H](9) + φ[C_η–C_α–C_β](7) + ν[C_δ–C_η](7)
1031	–	1036	–	φ[C_β–C_γ–H](20) + ν[C_δ–C_η](15) + φ[C_δ–C_η–H](7) + φ[C_δ–C_ε–H](9) + φ[H–C_α–C_β](7) + φ[C_δ–C_η–H](7) + φ[H–C_η–C_α](7) + φ[C_η–C_α–H](5)	1026	–	1036	–	φ[C_η–C_α–H](37) + φ[H–C_α–C_β](33) + φ[C_β–C_γ–H](7) + ν[C_δ–C_ε](5) + φ[H–C_η–C_α](5)
1017	–	1018	–	ν[C_η–C_α](43) + φ[C_η–C_α–H](14) + φ[C_δ–C_η–C_α](11) + φ[C_η–C_α–C_β](10) + φ[H–C_η–C_α](9)	1006	–	1018	–	φ[C_β–C_γ–H](29) + φ[C_η–C_α–H](15) + φ[C_δ–C_η–H](10) + φ[C_δ–C_ε–H](9) + φ[C_α–C_β–C_γ](6)ν[C_β–C_γ](6)
972	–	978	–	φ[C_β–C_γ–H](23) + ν[C_β–C_γ](20) + ν[C_δ–C_ε](18) + φ[C_η–C_α–H](14) + φ[H–C_η–C_α](6)	986	–	978	962	ν[C_η–C_α](28) + φ[C_η–C_α–H](16) + ν[C_δ–C_ε](14) + ν[C_β–C_γ](11) + φ[H–C_η–C_α](9) + φ[H–C_α–C_β](6)
954	–	943	–	φ[C_β–C_γ–H](82)	954	–	943	–	φ[H–C_α–C_β](6)
886	896	–	890	φ[C_δ–C_ε–H](49) + φ[C_β–C_γ–H](25) ν[C_α–C_β](8)	900	896	–	890	φ[C_β–C_γ–H](47) + φ[C_δ–C_ε–H](12) + ν[C_α–C_β](7) + φ[H–C_α–C_β](7)
877	880	–	–	φ[C_δ–C_ε–H](64) + φ[C_β–C_γ–H](19)	878	880	–		φ[C_δ–C_ε–H](88)
817	803	–	845	φ[C_δ–C_ε–H](55) + ν[C_δ–C_η](15) + ν[C_α–C_β](8)	836	803	–	845	φ[C_δ–C_ε–H](69) + ν[C_δ–C_η](7)
787	–	782	–	φ[H–C_α–C_β](36) + φ[C_δ–C_η–H](31) + φ[C_η–C_α–H](6)	777	–	782	–	φ[H–C_α–C_β](39) + ν[C_β–C_γ](19) + φ[C_δ–C_η–H](18) + φ[C_η–C_α–H](8) + ν[C_δ–C_ε](6)
764	760	–	759	φ[H–C_α–C_β](18) + φ[C_η–C_α–C_β](13) + ν[C_β–C_γ](13) + φ[C_δ–C_η–C_α](12) + ν[C_α–C_β](6) + φ[C_δ–C_η–H](5) + φ[C_η–C_α–H](5)	736	760	–	759	φ[C_δ–C_η–H](43) + φ[H–C_η–C_α](11) +φ[H–C_α–C_β](10) + φ[C_η–C_α–H](10) +τ[C_η–C_α](8) + τ[C_δ–C_η](6) + τ[C_α–C_β](5)
729	–	750	–	φ[C_δ–C_η–H](39) + ν[C_δ–C_ε](11) + φ[H–C_η–C_α](10) + φ[H–C_α–C_β](7) + τ[C_η–C_α](7) + φ[C_η–C_α–H](7)	639	–	750	–	ν[C_δ–C_η](37) + ν[C_δ–C_ε](20) + ν[C_β–C_γ](13) + ν[C_β=C_δ](8) + ν[C_α–C_β](7)
515	–	580	–	ν[C_β–C_γ](20) + ν[C_δ–C_ε](15) + τ[C_δ–C_ε](14) + φ[C_α–C_β=C_δ](10) + φ[C_β=C_δ–C_ε](9) + φ[C_β=C_δ–C_η](5)	544	–	580	–	φ[C_δ–C_η–C_α](24) + ν[C_α–C_β](16) + φ[C_α–C_β–C_γ](9) + φ[C_η–C_α–C_β](9) + φ[C_ε–C_δ–C_η](8) + φ[C_γ–C_β=C_δ](6)

Table 3 continued

Cal. freq.	Obs. freq. IR[a]	Raman[a]	IR[b]	Assignment (% PED) ($\delta = 0$)	Cal. freq.	Obs. freq. IR[a]	Raman[a]	IR[b]	Assignment (% PED) ($\delta = \pi$)
484	–	489	–	$\tau[C_\delta–C_\varepsilon](74) + \varphi[C_\delta–C_\eta–C_\alpha](6)$	496		489		$\tau[C_\delta–C_\varepsilon](81) + \varphi[C_\eta–C_\alpha–C_\beta](7) + \varphi[C_\delta–C_\eta–C_\alpha](5)$
456	454	–	–	$\varphi[C_\alpha–C_\beta–C_\gamma](23) + \varphi[C_\varepsilon–C_\delta–C_\eta](12) + \varphi[C_\beta{=}C_\delta–C_\eta](8) + \varphi[C_\gamma–C_\beta{=}C_\delta](8) + \nu[C_\delta–C_\varepsilon](8) + \varphi[C_\eta–C_\alpha–C_\beta](8) + \tau[C_\delta–C_\varepsilon](7) + \varphi[C_\delta–C_\eta–C_\alpha](7)$	461	454	–	–	$\varphi[C_\alpha–C_\beta{=}C_\delta](17) + \varphi[C_\beta{=}C_\delta–C_\varepsilon](16) + \varphi[C_\beta{=}C_\delta–C_\eta](11) + \nu[C_\beta–C_\gamma](11) + \nu[C_\delta–C_\eta](9) + \nu[C_\delta–C_\varepsilon](7) + \nu[C_\alpha–C_\beta](9) + \varphi[C_\gamma–C_\beta{=}C_\delta](9)+$
402	–	415	–	$\varphi[C_\delta–C_\eta–C_\alpha](30) + \varphi[C_\eta–C_\alpha–C_\beta](29) + \varphi[C_\alpha–C_\beta–C_\gamma](9) + \tau[C_\beta–C_\gamma](7)$	393	–	415	–	$\varphi[C_\delta–C_\eta–C_\alpha](35) + \varphi[C_\alpha–C_\beta–C_\gamma](17) + \varphi[C_\eta–C_\alpha–C_\beta](11) + \tau[C_\delta–C_\varepsilon](10) + \varphi[C_\gamma–C_\beta{=}C_\delta](5)$
331	407	–	–	$\varphi[C_\varepsilon–C_\delta–C_\eta](27) + \tau[C_\delta–C_\eta](18) + \tau[C_\alpha–C_\beta](15) + \varphi[C_\alpha–C_\beta–C_\gamma](13) + \varphi[C_\beta{=}C_\delta–C_\varepsilon](9) + \varphi[C_\beta{=}C_\delta–C_\eta](6)$	360	407	–	–	$\varphi[C_\eta–C_\alpha–C_\beta](31) + \tau[C_\alpha–C_\beta](11) + \tau[C_\delta–C_\eta](10) + \nu[C_\alpha–C_\beta](9) + \varphi[C_\alpha–C_\beta–C_\gamma](6) + \tau[C_\beta–C_\gamma](6)$
262	260	–	–	$\tau[C_\beta–C_\gamma](91)$	319	260	–	–	$\varphi[C_\varepsilon–C_\delta–C_\eta](35) + \varphi[C_\alpha–C_\beta–C_\gamma](18) + \varphi[C_\beta{=}C_\delta–C_\eta](9) + \varphi[C_\beta{=}C_\delta–C_\varepsilon](8)$
216	215	–	–	$\varphi[C_\beta{=}C_\delta–C_\varepsilon](31) + \varphi[C_\beta{=}C_\delta–C_\eta](17) + \varphi[C_\alpha–C_\beta{=}C_\delta](15) + \varphi[C_\gamma–C_\beta{=}C_\delta](14) + \tau[C_\eta–C_\alpha](7) + \tau[C_\delta–C_\eta](6)$	216	215	–	–	$\tau[C_\beta–C_\gamma](92)$
214	–	150	–	$\varphi[C_\gamma–C_\beta{=}C_\delta](16) + \tau[C_\alpha–C_\beta](12) + \nu[C_\delta–C_\eta](12) + \nu[C_\alpha–C_\beta](11) + \varphi[C_\eta–C_\alpha–C_\beta](8) + \varphi[C_\delta–C_\eta–C_\alpha](8) + \tau[C_\delta–C_\eta](7) + \varphi[C_\alpha–C_\beta{=}C_\delta](6)$	214	–	150	–	$\varphi[C_\beta{=}C_\delta–C_\varepsilon](19) + \varphi[C_\gamma–C_\beta{=}C_\delta](16) + \tau[C_\alpha–C_\beta](14) + \tau[C_\delta–C_\eta](14) + \varphi[C_\eta–C_\alpha–C_\beta](6) + \varphi[C_\alpha–C_\beta{=}C_\delta](6)$
119	–	125	–	$\tau[C_\alpha–C_\beta](27) + \tau[C_\delta–C_\eta](15) + \nu[C_\alpha–C_\beta](7) + \varphi[C_\varepsilon–C_\delta–C_\eta](7) + \varphi[C_\beta{=}C_\delta–C_\eta](7) + \nu[C_\delta–C_\eta](6) + \varphi[C_\alpha–C_\beta–C_\gamma](7) + \varphi[C_\alpha–C_\beta{=}C_\delta](6)$	119	–	125	–	$\varphi[C_\beta{=}C_\delta–C_\varepsilon](18) + \varphi[C_\alpha–C_\beta{=}C_\delta](17)\tau[C_\alpha–C_\beta](16) + \tau[C_\delta–C_\eta](15) + \varphi[C_\gamma–C_\beta{=}C_\delta](9) + \varphi[C_\beta{=}C_\delta–C_\varepsilon](8)$

All frequencies are in cm^{-1}

[a] Observed IR and Raman frequencies are from ref. [13]

[b] Observed IR frequencies are from ref. [12]

Only dominant PED's are given

two CH_2 groups to be at 1331 and 1223 cm^{-1}. The two twisting modes of CH_2 groups are calculated at 1102 and 1057 cm^{-1} and are matched to the peaks 1095 and 1050 cm^{-1}, respectively. These modes approach each other and reach 1096 and 1065 cm^{-1} at the zone boundary. As the phase angle advances, the 1102 cm^{-1} mode retains its purity of character present at the zone center whereas the mode 1057 cm^{-1} which has a twisting character at the zone center slowly transfers this character into 1031 cm^{-1} mode. At the zone boundary the 1031 cm^{-1} mode becomes purely a twist mode where as the other becomes a mixed one comprising of various stretches and angle bends of the back bone. The rocking modes of CH_2 groups are calculated at 787, 764, and 729 cm^{-1}. The mode at 787 cm^{-1} consists of rocking of both the CH_2 groups. As the phase factor advances the backbone, stretch v $[C_\beta–C_\gamma]$ starts mixing in this mode and the mode disperses a little. This mode takes a constant value around $\delta = 0.4\pi$. The other two twisting modes at 764 and 729 cm^{-1} come closer to each other and suffer a weak repulsion. A comparison of modes of CH_2 group in different polymers is given in Table 6. This basically shows that CH_2 frequencies are of group character. The mode which appears at 263 cm^{-1} at the zone center is a torsion mode. Initially it is non dispersive in nature. It suffers repulsion twice, first around $\delta = 0.4\pi$ and second around $\delta = 0.6\pi$. As expected, the repulsion is accompanied by the exchange of characters. These values may be points of internal symmetry and have regions of high density of states. The fluctuating scatterings in the Raman spectra [16] in the region of 300 wave numbers may be because of the presence of the regions of high density of states.

Characteristic features of the dispersion curves

The dispersion curves of PDMB have been obtained for a linear isolated chain. The evaluation of dispersion curves for a three dimensional (3D) system is somewhat involved

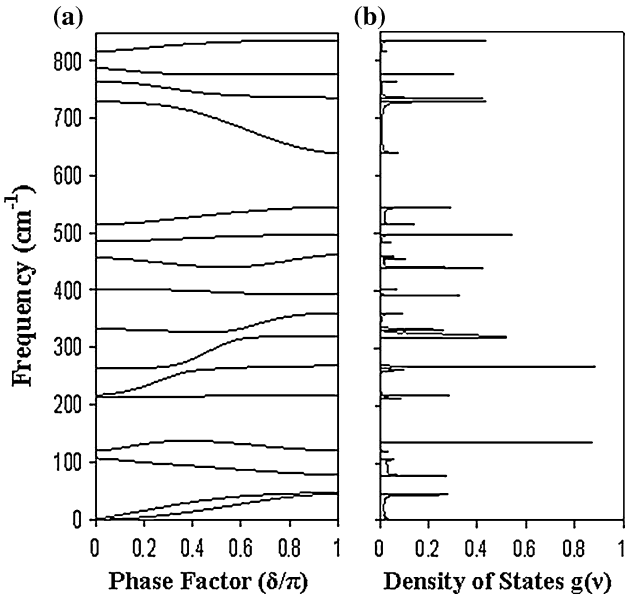

Fig. 2 **a** Dispersion curves of PDMB (0–850 cm^{-1}). **b** Density-of-states of PDMB (0–850 cm^{-1})

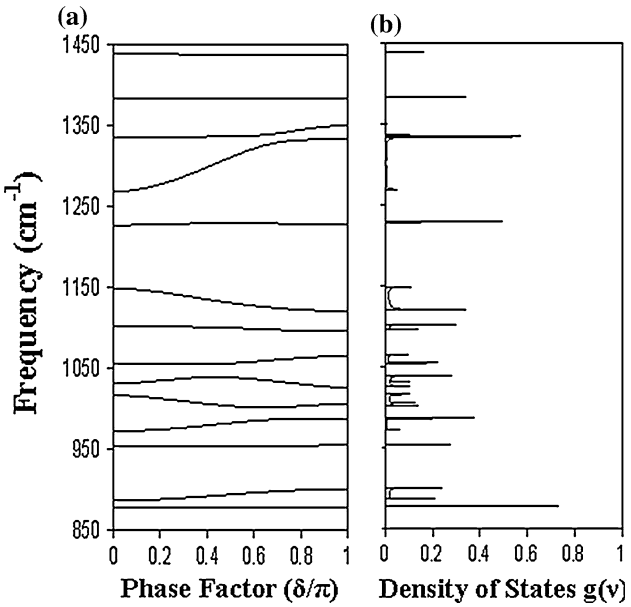

Fig. 3 **a** Dispersion curves of PDMB (850–1450 cm^{-1}). **b** Density-of-states of PDMB (850–1450 cm^{-1})

in terms of both dimensions and a large number of interactions. It is not easy to solve the problem without first solving it for a linear isolated chain. This alone can provide the best starting point. It has been generally observed that the intramolecular interactions (covalent and non bonded) are generally stronger than the intermolecular interactions (hydrogen bonding and non bonded). Crystal field only leads to splitting near the zone center and zone boundary. The basic profile of the dispersion curves remains more or less unaltered. Thus, the study of phonon dispersion in polymeric systems is an important study.

A close examination of dispersion curves shows that those corresponding to Ag species are less dispersive where as those belonging to Au species show appreciable dispersion.

One of the prominent features of dispersion curves is the repulsion and exchange of character between various pairs of modes. The pair of modes, which show repulsion, are listed in Table 7 along with their PED's before and after the exchange of characters between them. To ascertain whether it is a crossing or a repulsion, calculations at very close intervals of $\delta = 0.001\pi$ have been performed for all pairs and it was found that there was a repulsion. The interesting phenomenon of exchange of character may be classically viewed as a collision in the energy momentum space (ε, p) of two phonons approaching each other and moving apart after exchanging their energies.

The dispersion curves at 1031, 1017, 456, and 120 cm^{-1} have flat regions indicating high density of states. The presence of regions of high density of states also refers to some internal symmetry points in the energy momentum space and is known as van Hove type singularities [27]. These are listed in Table 8. The mode at 1031 cm^{-1} exhibits a high density of states region at around $\delta = 0.45\pi$. The mode at 1017 cm^{-1} is mainly a stretching mode $\nu[C_\eta–C_\alpha]$ (43%). As the phase factor advances, the contribution of this stretch $\nu[C_\eta–C_\alpha]$ decreases and of angle bend $\varphi[C_\beta–C_\gamma–H]$ increases with that of angle bend $\varphi[H–C_\eta–C_\alpha]$ remaining almost constant. It shows a high density of states at $\delta = 0.7\pi$. The other two modes at 456 and 120 cm^{-1} exhibiting high density of states regions are skeletal and torsion modes. No crossing is present in the dispersion profile of the modes indicating a lack of the mirror plane of symmetry.

Out of the four acoustical modes, two modes do not resolve well away from the zone center. This is because the effective force constants involved in translational and rotational motions are very low.

Frequency distribution function and heat capacity

From the dispersion curves, frequency distribution function has been obtained and plotted in Figs. 2b and 3b. The peaks correspond to the regions of high density of states. The frequency distribution function can be used to calculate the thermo dynamical properties such as heat capacity, enthalpy, entropy, etc. In this study, it was used to obtain heat capacity of PDMB as a function of temperature. The predictive values of the heat capacity in the temperature range 10–400 K are shown in Fig. 4. The heat capacity variation is typical of an one-dimensional system, which has a large variation initially, but later on, it slows down. It may be added that the 3D

Table 4 Comparison of CH_3 modes in different polymers

CH_3 modes	PDMB IR/R	iP4MPI[a] IR	sP4MPI[a] IR	sPP[b] (helical) IR	sPP[b] (all *trans*) IR	iPP[b] IR	sPB[c] IR	iPB[c] IR
Asym. stretching	2980^{R}, 2970^{IR}	2961	2960	2959	2959	2956	2959	2961, 2958
Degenerate stretching	2918^{IR}, 2910^{R}	2882	2875	2882	2880	2880	2874	2874
Degenerate defor.	1463^{IR}, 1462^{R}, 1445^{IR}	1469	1464	1465	1466	1459	1463	1463, 1458
Sym. deform.	1377^{R}, 1331^{R}	1384, 1368	1375	1379	1381	1377, 1359	1388	1380
Rocking	943^{R}, 896^{IR}, 880^{IR}, 803^{IR}	1009, 918	1005, 988, 920	977, 870	972, 867	997, 973	1027, 972, 924	1062, 972, 924

All frequencies are in cm^{-1}

R and IR marked frequencies are observed only in Raman and IR spectra, respectively

sP4MPI syndiotactic poly(4-methyl-1-pentene), *iP4MPI* isotactic poly(4-methyl-1-pentene), *sPP* syndiotactic poly(propylene) form II, *iPP* isotactic poly(propylene), *sPB* syndiotactic poly(1-butene), *iPB* isotactic poly(1-butene)

[a] Ref. [24]

[b] Ref. [25]

[c] Ref. [26]

Table 5 Comparison of assignments of this study with that of Petcavich and Coleman study [13]

Obs. freq			This study		Petcavich and Colemen study	
IR[a]	Raman[a]	IR[b]	Cal. freq.	Assignments	Cal. freq.	Assignments
	1331		1336	CH_3 symmetric deformation	1299	CH_2 wagging
1260			1269	C–C stretches + H–C–C bendings	1316	CH_2 twisting
1155		1151	1149	CH_2 wagging	1163	C–C stretch + CH_3 asym. def.
1095			1102	CH_2 twisting	1074	C–C stretch + CH_3 rocking
1050			1057	CH_2 twisting	1031	CH_3 rocking
	978		972	CH_2 twisting	966	CH_3 rocking+ CH_2 rocking
	943		954	CH_3 rocking	946	CH_2 rocking+ CH_3 rocking
896		890	886	CH_3 rocking	925	CH_3 rocking+ CH_2 rocking
	782		787	Rocking CH_2	779	CH_2 rocking+ CH_3 rocking
	489		485	C–C torsion	495	C–C stretch+ C–C–C bending
	415		402	C–C–C bendings	287	C=C–C bendings
260			263	C–C torsion	242	C–C–C bending
215			217	C=C–C bendings	206	C–C–C bending+ C=C torsion

All frequencies are in cm^{-1}

[a] Observed IR and Raman frequencies are from ref. [13]

[b] Observed IR frequencies are from ref. [12]

picture, especially the lattice modes are not considered in this study. This problem is very difficult not only in terms of prohibitive dimensionality but also in terms of potential field. Many interactions would be even difficult to visualize. In spite of several such limitations involved in the vibrational dynamics and concomitant thermodynamic behavior of polymeric systems, the work on an isolated chain is always an useful starting point. Although the heat capacity is predictive in nature but it may stimulate some worker to carry out measurements at a later date.

Conclusions

The spectral data for the polymer PDMB have been satisfactorily interpreted from the vibration dynamics based on

Table 6 Comparison of CH_2 modes in different polymers

CH_2 modes	PDMB IR/R	PHB[a] IR/R	sPP[b] IR	iPP[b] IR	iPB[c] IR	sPB[c] IR	PE[a] IR/R
Asymmetric stretching	2948^{IR}, 2910^{R}	2933^{IR}, 2930^{R}	2926	2925	2914	2918	2919^{IR}, 2883^{R}
Symmetric stretching	2860^{IR}, 2855^{R}	2873^{IR}, 2873^{R}	2856	2868	2851	2866	2851^{IR}, 2848^{R}
Scissoring	1445^{IR}, 1438^{R}	1443^{R}	1455, 1450	1454	1441 1439	1463(b) 1463(s)	1473^{IR}, 1416^{R}
Wagging	1155^{IR}, 1018^{R}	1345^{R}	1350	1378, 1305	1342, 1302 1366, 1321	1353, 1286(b) 1313(s)	1370^{R}, 1175^{IR}
Twisting	1095^{IR}, 1050^{IR}	1278^{IR}, 1261^{R}	1200, 1226	1219, 1239	1222, 1207 1263	1163, 1074(b) 1265, 1108(s)	1296^{R}, 1050^{IR}
Rocking	782^{R}, 760^{IR}, 750^{R}	825^{IR}, 840^{R}	831, 829	841, 807	816, 798 764, 758	883, 807(b) 781, 753(s)	$1170^{R,}$ 734^{IR}

All frequencies are in cm^{-1}

R and IR marked frequencies are observed only in Raman and IR spectra, respectively

PHB poly(β-hydroxybutyrate)-α form, *sPP* syndiotactic poly(propylene) form II (all *trans*), *iPP* isotactic poly(propylene), *iPB* isotactic poly (1-butene), *sPB* syndiotactic poly(1-butene), *PE* polyethylene

[a] Ref. [8]

[b] Ref. [25]

[c] Ref. [26]

Table 7 Pair of modes that repel and exchange of character

Freq. ($\delta = 0$)	Before exchange				After exchange		
	δ^a/π	δ^b/π	Freq.	PED	δ^b/π	Freq.	PED
1336	0.70	0.65	1339	φ[H–C_ε–H](34) + φ[C_δ–C_ε–H](30) + ν[C_δ–C_ε](10) + ν[C_α–C_β](6)	0.75	1349	ν[C_η–C_α](12) + ν[C_α–C_β](13) + φ[H–C_ε–H](17) + φ[C_δ–C_ε–H](15) + φ[C_η–C_α–H](7) + φ[H–C_η–H](7) + φ[C_δ–C_η–H](5) + ν[C_δ–C_ε](7)
1269	0.70	0.65	1326	ν[C_η–C_α](16) + ν[C_α–C_β](13) + φ[H–C_ε–H](13) + φ[C_δ–C_ε–H](11) + φ[C_η–C_α–H](9) + φ[H–C_η–H](7) + φ[C_δ–C_η–H](7) + φ[H–C_α–C_β](6)	0.75	1332	φ[H–C_ε–H](30) + φ[C_δ–C_ε–H](27)ν[C_α–C_β](6) + ν[C_η–C_α](9)
764	0.35	0.20	759	φ[C_η–C_α–C_β](13) + φ[C_δ–C_η–C_α](12) +φ[C_δ–C_η–H](11)+φ[H–C_α–C_β](10) + ν[C_α–C_β](8) + ν[C_δ–C_η](7) + ν[C_β–C_γ](9)	0.50	742	φ[C_δ–C_η–H](39) + φ[H–C_η–C_α](9)φ[H–C_α–C_β](8) + φ[C_η–C_α–H](8) + τ[C_δ–C_η](6)
729	0.35	0.20	726	φ[C_δ–C_η–H](34) + φ[H–C_η–C_α](8) + φ[H–C_α–C_β](7) + φ[C_η–C_α–H](6)ν[C_δ–C_η](6) + τ[C_δ–C_η](6) + ν[C_δ–C_ε](12)	0.50	699	φ[C_η–C_α–C_β](8)+φ[C_δ–C_η–C_α](8)φ[C_δ–C_η–H](9) + ν[C_α–C_β](12) + ν[C_δ–C_η](21) + ν[C_δ–C_ε](13)
332	0.60	0.50	327	φ[C_ε–C_δ–C_η](20) + φ[C_α–C_β–C_γ](17) +φ[C_β=C_δ–C_α](11) + τ[C_α–C_β](10) + τ[C_δ–C_η](7) + τ[C_β–C_γ](5)	0.70	345	ν[C_α–C_β](12) + φ[C_η–C_α–C_β](25) + τ[C_δ–C_η](7) + τ[C_β–C_γ](5) + τ[C_α–C_β](10) + φ[C_α–C_β–C_γ](10) + τ[C_α–C_β](10) + φ[C_α–C_β–C_γ](10) + ν[C_δ–C_η](7) + φ[C_α–C_β=C_δ](6)
263	0.60	0.50	300	ν[C_α–C_β](14) + φ[C_β=C_δ–C_ε](13) + φ[C_ε–C_δ–C_η](9) + ν[C_δ–C_η](9) + φ[C_η–C_α–C_β](8) + τ[C_β–C_γ](8) + φ[C_α–C_β=C_δ](7) + τ[C_δ–C_η](7) + φ[C_δ–C_η–C_α](6)	0.70	318	φ[C_ε–C_δ–C_η](34) + φ[C_α–C_β–C_γ](14) + φ[C_β=C_δ–C_η](12) + τ[C_δ–C_η](7) + φ[C_β=C_δ–C_ε](6)

Table 7 continued

Freq. ($\delta = 0$)	Before exchange				After exchange		
	δ^a/π	δ^b/π	Freq.	PED	δ^b/π	Freq.	PED
263	0.40	0.25	265	$\tau[C_\beta–C_\gamma](84)$	0.45	290	$\varphi[C_\beta{=}C_\delta–C_\eta](12) + \varphi[C_\alpha–C_\beta{=}C_\delta](7) + \nu[C_\delta–C_\eta](9)+\nu[C_\alpha–C_\beta](14) + \tau[C_\beta–C_\gamma](13) + \varphi[C_\eta–C_\alpha–C_\beta](9) + \varphi[C_\delta–C_\eta–C_\alpha](6)$
217	0.40	0.25	240	$\varphi[C_\beta{=}C_\delta–C_\eta](11) + \varphi[C_\alpha–C_\beta{=}C_\delta](11) + \varphi[C_\beta{=}C_\delta–C_\varepsilon](10) + \nu[C_\delta–C_\eta](10) + \nu[C_\alpha–C_\beta](10) + \varphi[C_\gamma–C_\beta{=}C_\delta](9) + \varphi[C_\delta–C_\eta–C_\alpha](5)$	0.45	261	$\tau[C_\beta–C_\gamma](80) + \varphi[C_\eta–C_\alpha–C_\beta](6)$

δ^a corresponds to repulsion points. δ^b corresponds to the points before/after repulsion

Table 8 Flat regions

Freq. ($\delta = 0$)	δ/π	Freq.	% PED	Freq. ($\delta = 0$)	δ/π	Freq.	% PED
1031	0.45	1039	$\varphi[C_\eta–C_\alpha–H](19) + \varphi[H–C_\alpha–C_\beta](16) + \varphi[C_\beta–C_\gamma–H](12) + \nu[C_\eta–C_\alpha](8) + \varphi[C_\delta–C_\eta–H](7) + \nu[C_\delta–C_\eta](6)$	1017	0.70	1002	$\varphi[C_\beta–C_\gamma–H](24) + \varphi[C_\eta–C_\alpha–H](17) + \nu[C_\eta–C_\alpha](9) + \varphi[H–C_\eta–C_\alpha](8) + \varphi[C_\delta–C_\varepsilon–H](8) + \varphi[H–C_\varepsilon–H](6)$
456	0.55	440	$\varphi[C_\alpha–C_\beta–C_\gamma](20) + \varphi[C_\gamma–C_\beta{=}C_\delta](13) + \varphi[C_\beta{=}C_\delta–C_\varepsilon](19) + \varphi[C_\varepsilon–C_\delta–C_\eta](9) + \varphi[C_\beta{=}C_\delta–C_\eta](8) + \varphi[C_\alpha–C_\beta{=}C_\delta](7)\nu[C_\delta–C_\eta](6) + \nu[C_\delta–C_\varepsilon](6)$	120	0.40	137	$\tau[C_\alpha–C_\beta](20) + \tau[C_\beta{=}C_\delta](17) + \varphi[C_\beta{=}C_\delta–C_\eta](11) + \varphi[C_\alpha–C_\beta{=}C_\delta](10) + \varphi[C_\beta{=}C_\delta–C_\varepsilon](7) + \varphi[C_\gamma–C_\beta{=}C_\delta](7) + \tau[C_\eta–C_\alpha](6)$

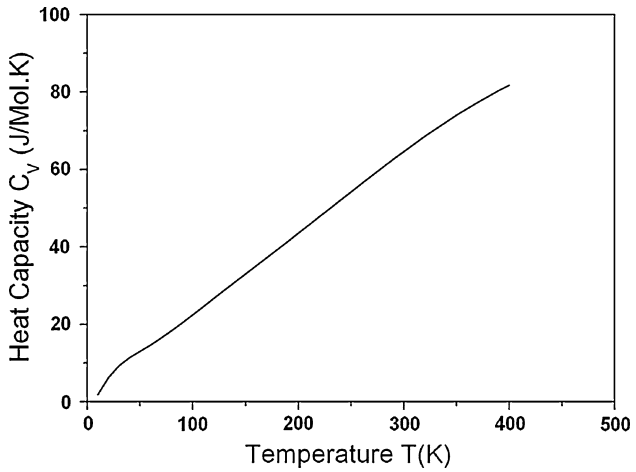

Fig. 4 Variation of heat capacity Cv with temperature

UBFF and the profile of dispersion curves. The characteristic features of the dispersion curves such as the regions of high density of states, repulsion and exchange of characters are well interpreted. In addition, the predictive values of specific heat show a typical variation for an one-dimensional polymeric system.

References

1. Hu S, Smith KM, Spiro TG (1996) J Am Chem Soc 118:12638
2. Dong S, Spiro TG (1998) J Am Chem Soc 120:10434
3. Applications of fourier transform Raman spectroscopy: Hendra PJ (guest editor) 1990. University of Southampton, U.K. 4–6 April 1990. Special edition. Spectrochim Acta 46A(2):121–337
4. Painter PC, Coleman MM, Koenig JL (1982) The theory of vibrational spectroscopy and its applications to polymeric material. Wiley, New York
5. Gupta A, Choudhary N, Bee S, Tandon P, Gupta VD (2010) Polym Sci Ser A 52:1057
6. Kumar N, Shukla SK, Tandon P, Gupta VD (2009) J Polym Sci Part B Polym Phys 47:2353
7. Singh M, Kumar A, Kumar N, Tandon P, Gupta VD (2009) Chem Chem Tech 3:7
8. Chaturvedi D, Mishra S, Tandon P, Gupta VD, Siesler WH (2009) Polym Engg Sci 49:850
9. Brydson JA (1978) Rubber chemistry. Applied Science Publishers, London, p 4
10. Long LC (2001) Rubber Chem Technol 74:493
11. Chatani Y, Nakatani S (1972) Macromolecules 5:597
12. Miyata M, Morioka K, Takemoto K (1977) J Polym Sci Polym Chem Ed 15:2987
13. Ichikawa T, Nakao O, Suzuki T, Okazaki T, Ohta N (1986) Int J Radiat Appl Instrum Part C Radiat Phys Chem 28:295
14. Ichikawa T, Nakao O, Ohta N (1987) Int J Radiat Appl Instrum Part C Radiat Phys Chem 29:435

15. Cataldo F, Ragni P, Ursini O, Angelini G (2008) Radiat Phys chem 77:941
16. Petcavich RJ, Coleman MM (1980) J Polym Sci 18:2097
17. Urey HC, Bradley HC (1931) Phys Rev 38:1969
18. Wilson EB, Decius JC, Cross PC (1980) Molecular vibrations: the theory of infrared and Raman vibrational spectra. Dover Publications, New York
19. Higgs PW (1953) Proc R Soc Lond A 220:472
20. Mannfors B, Palmo K, Krimm S (2000) J Mol Struct 556:1
21. Pathak A, Saxena V, Tandon P, Gupta VD (2006) Polymer 47:5154
22. Kings WT, Mills IM, Crawford BL (1957) J Chem Phys 27:475
23. Petcavich RJ, Coleman MM (1980) J Macromol Sci Phys B18:47
24. Pande S, Kumar A, Tandon P, Gupta VD (2001) Vib Spectrosc 26:161
25. Saxena V, Mishra RM, Tandon P, Gupta VD (2005) Polymer 46:7386
26. Sharma P, Tandon P, Gupta VD (2000) Eur Polym J 36:2629
27. Callaway J (1974) Quantum theory of solids. Academic Press, New York and London